Reaction Mechanisms

Deutsche Ausgabe: DOI: 10.1002/ange.201607230
Internationale Ausgabe: DOI: 10.1002/anie.201607230

Insights into the Reaction Mechanism of Ethanol Conversion into Hydrocarbons on H-ZSM-5

Kristof Van der Borght[+], Rakesh Batchu[+], Vladimir V. Galvita, Konstantinos Alexopoulos, Marie-Françoise Reyniers, Joris W. Thybaut, and Guy B. Marin*

Abstract: *Ethanol dehydration to ethene is mechanistically decoupled from the production of higher hydrocarbons due to complete surface coverage by adsorbed ethanol and diethyl ether (DEE). The production of C_{3+} hydrocarbons was found to be unaffected by water present in the reaction mixture. Three routes for the production of C_{3+} hydrocarbons are identified: the dimerization of ethene to butene and two routes involving two different types of surface species categorized as aliphatic and aromatic. Evidence for the different types of species involved in the production of higher hydrocarbons is obtained via isotopic labeling, continuous flow and transient experiments complemented by UV/Vis characterization of the catalyst and ab initio microkinetic modeling.*

Direct catalytic upgrading of alcohols into chemicals has the potential to be a sustainable production route.[1] The zeolite catalyzed conversion of methanol is the most extensively investigated but ethanol conversion is gaining interest rapidly.[2] In ethanol conversion, most research focuses on catalyst improvement via post-synthesis treatment,[3] phosphorus addition,[4] and metal modification,[5] but only few mechanistic studies are available.[6] Three rivalling mechanisms have been proposed for the conversion of ethanol to C_{3+} hydrocarbons on H-ZSM-5: an acid-catalyzed reaction mechanism with ethene as primary product of a fast dehydration reaction and subsequent production of higher hydrocarbons requiring the coupling of ethene,[7] a radical-assisted mechanism,[8] and a dual cycle mechanism[9] analogous to the one proposed for the methanol-to-olefins process.[1] The latter comprises an aromatic-assisted mechanism for the production of ethene and propene (arene-based cycle), and a methylation/cracking cycle for the production of higher olefins. This was confirmed by both experimental[10] and theoretical[11] studies. Different types of surface intermediates, such as carbenes, have been observed during MTO.[12] The dual cycle mechanism, however, fails in explaining important experimental observations such as the first carbon–carbon coupling and the reversibility of the reaction.[13]

Herein, a detailed reaction mechanism is proposed for the conversion of ethanol to hydrocarbons, consisting of two consecutive stages as illustrated in Figure 1. The first stage in ethanol conversion involves the dehydration of ethanol to ethene, which can take place either via a monomolecular or a bimolecular pathway with diethyl ether (DEE) as intermediate product. In the second stage, three consecutive routes for the production of light olefins can be distinguished which are mediated by different types of surface intermediates: butene formation via alkylation of adsorbed ethene (C_2H_4*) with gas phase ethene (Route I) and formation of propene and butene via two different types of surface species. The surface species are not only aromatics, that is, C^*_{aro}, typically referred to as the hydrocarbon pool in methanol-to-olefins, which allow enhanced production of light olefins (Route III) via paring and side-chain reaction mechanisms comparable to the arene-based cycle, but also shorter-lived aliphatic species, that is, C^*_{ali}, which can undergo β-scission, isomerization and alkylation (Route II). There is competition between the routes to propene and/or butenes mediated by these two types of intermediates, which depends on the

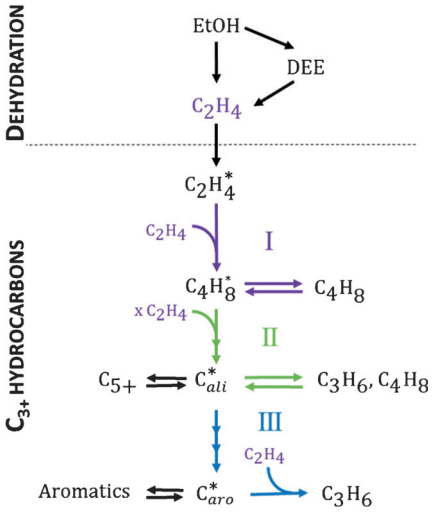

Figure 1. Reaction mechanism proposed in this work for the conversion of ethanol to hydrocarbons,. EtOH: ethanol, DEE: diethyl ether, C_2H_4: ethene, C_3H_6: propene, C_4H_8: butene, C_{5+}: olefinic hydrocarbons containing more than five carbon atoms, aromatics: hydrocarbons containing one or more aromatic rings, C_2H_4*: ethene surface species; C_4H_8*: butene surface species; C^*_{ali}: aliphatic surface species, C^*_{aro}: aromatic surface species. Route I (violet): dimerization of ethene to butene, Route II (green): formation of propene and butene via aliphatic surface intermediates, Route III (blue): formation of propene via aromatic surface intermediates.

[*] K. Van der Borght,[+] R. Batchu,[+] Dr. V. V. Galvita, Dr. K. Alexopoulos, Prof. M.-F. Reyniers, Prof. J. W. Thybaut, Prof. G. B. Marin
Laboratory for Chemical Technology, Ghent University
Technologiepark 914, 9052 Gent (Belgium)
E-mail: Vladimir.Galvita@ugent.be

[+] These authors contributed equally to this work.

Supporting information and the ORCID identification number(s) for the author(s) of this article can be found under: http://dx.doi.org/10.1002/anie.201607230.

reaction conditions. Furthermore, water has no effect on the subsequent conversion to higher hydrocarbons. This mechanism is supported by evidence obtained from continuous flow and transient experiments combined with quantum chemical calculations on the dehydration of ethanol and the consecutive oligomerization of ethene. The nature of the surface species was derived from isotope labeled transient experiments and UV/Vis spectroscopy characterization.

Continuous-flow experiments for investigation of the steady-state behavior with varying site time at 573 K are shown in Figure 2a. It is clear that below a site time of 1.0 $mol_{H^+}\,s\,mol^{-1}$, ethanol dehydration is incomplete and both diethyl ether and ethene are produced. Higher hydrocarbon formation, quantified by the C_2 conversion, which is the combined conversion of ethanol and ethene, is only observed at site times exceeding 1.5 $mol_{H^+}\,s\,mol^{-1}$. The role of the dehydration and the apparent decoupling between ethanol dehydration and higher hydrocarbon formation can be explained using density functional theory based microkinetic modeling of ethanol dehydration[14] and dimerization of ethene to 1-butene (Route I, Figure 1), which is the critical step in the formation of higher hydrocarbons. The full reaction network considered for these simulations is given in the Supporting Information, Figure S1. As illustrated in Figure 2b, the production of the higher hydrocarbons, here represented by 1-butene, only starts when ethanol conversion is almost complete. The surface coverages plotted in Figure 2c show that the catalyst surface is initially covered with adsorbed ethanol, which is rapidly replaced by adsorbed diethyl ether. The surface remains fully covered during dehydration. Free sites (*) for the adsorption of ethene and the production of higher hydrocarbons become available only at nearly complete ethanol conversion ($X_{EtOH} > 0.9$). The calculated dependency of the surface coverages on the site time can be explained by the pronounced differences of the equilibrium coefficients for adsorption (Supporting Information, Figure S2).

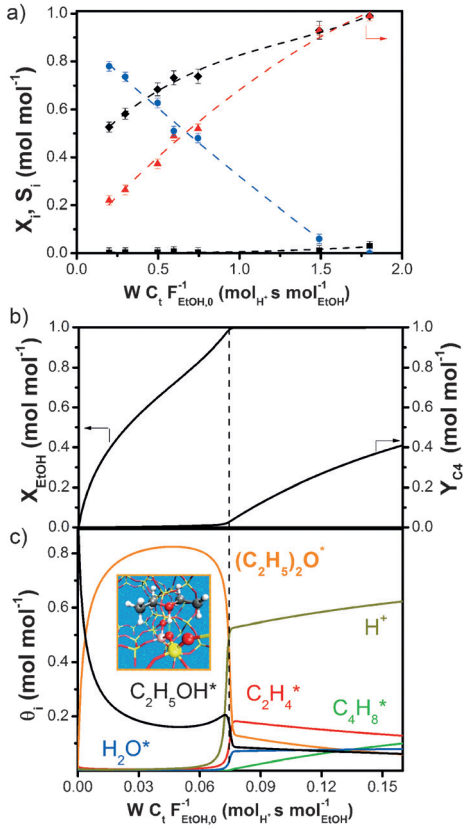

Figure 2. a) Ethanol conversion (◆, black), C_2 conversion (■, black), and selectivity to ethene (▼, red) and diethyl ether (○, blue) as function of site time. Lines are to guide the eye. b) Simulated ethanol conversion (X_{EtOH}) and butene yield (Y_{C4}) as function of site time using ab initio calculated rate and equilibrium coefficients and solving Equations S5–S7 of the Supporting Information. c) Corresponding simulated fractional surface coverages (the notation used for the adsorbed species is further clarified in the Supporting Information) as a function of site time; black: adsorbed ethanol ($C_2H_5OH^*$), red: adsorbed C_2H_4 ($C_2H_4^*$), orange: adsorbed diethyl ether ($(C_2H_5)O^*$), blue: adsorbed water (H_2O^*, green: adsorbed 1-butene ($C_4H_8^*$), khaki: free acid sites (*). ($T = 573$ K, $p_{EtOH,0} = 30$ kPa).

The conversion of ethanol into C_{3+} hydrocarbons, represented by the C_2 conversion, as function of site time in continuous flow experiments exhibits an induction period ($\tau_{ethanol}$), as shown in Figure 3, which is typical for an autocatalytic reaction mechanism. This phenomenon has already been reported for methanol conversion[15] but not for ethanol conversion. The same experiment but now with an ethene feed results in a shift of the site time–conversion curve to lower site time, that is, a decrease of the induction period. From Figure 3, the production rates of C_{3+} hydrocarbons from ethanol and ethene, taken as the slope in the conversion–site time curve beyond the induction period, can be calculated to be, respectively, $(9.1 \pm 1.1) \times 10^{-2}\,mol\,s^{-1}\,mol^{-1}$ and $(10.5 \pm 0.6) \times 10^{-2}\,mol\,s^{-1}\,mol^{-1}$, do not differ significantly. Although water inhibition during ethene conversion has been observed,[16] our observations indicate that the effect of water greatly depends on the operating conditions, as experiments with additional water to the feed show that the

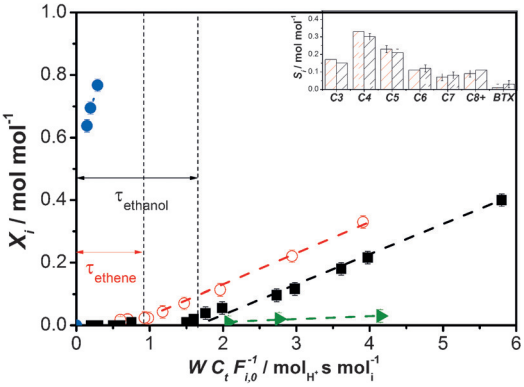

Figure 3. Conversion of different feeds: ethanol (C_2-conversion as defined in the Supporting Information, ■, black), ethene (○, red), propene (●, blue), and methanol (▼, green) as a function of site time. Inset: selectivity towards higher hydrocarbons (C_3–C_{8+}) and aromatics (benzene–toluene–xylenes) at $X_{C2} = 0.2$ for ethene (red) and ethanol (black) ($T = 573$ K, $p_{EtOH,MeOH,0} = 30$ kPa, $p_{C_2H_4,C_3H_6,0} = 27$ kPa). Lines are to guide the eye.

conversion is unaffected by this (see the Supporting Information). At 573 K, it can be concluded that apart from different induction periods no other difference exists in the conversion of ethanol or ethene to hydrocarbons.

The induction period observed in ethene conversion (τ_{ethene}) corresponds to the timescale on which the species responsible for autocatalysis are formed. The induction period observed in ethanol conversion is the sum of the time required for dehydration of ethanol and the time for formation of the autocatalytic species. This induction period was also observed at 593 K and 623 K (see the Supporting Information). However this was found to decrease with increasing temperature, which could be attributed to the increased rate of ethanol dehydration. The site time conversion behavior was found to be reversible, that is, when working at high site time, followed by a switch to a lower site time by increasing the flow rate and subsequently going back to the original site time, results in the same conversion (results not shown). This indicates that species that are formed and remain trapped inside the pores do not contribute significantly to the reaction.

The product distribution observed at 20% C_2 conversion in the continuous-flow experiments is shown as an inset in Figure 3. The primary products are olefins with carbon numbers up to ten and the selectivity towards aromatics is around 1%. Similar selectivities towards the different product classes are observed at the same C_2 conversion for ethanol and ethene feeds illustrating that the selectivity is unaffected by the presence of water due to ethanol dehydration. Propene and butenes have been identified as the primary C_{3+} hydrocarbon products for both ethanol and ethene feeds using a delplot analysis[17] (Supporting Information, Figure S6). Propene exhibits a much higher reactivity compared to ethanol and ethene (Figure 3), which can be attributed to the involvement of a secondary surface intermediate in the initiation step while the conversion of ethanol and ethene depends on the dimerization of ethene (Route I in Figure 1), which involves the formation of a less stable primary reaction intermediate. Methanol conversion remains fairly low (Figure 3) which is in accordance with results obtained by Qian et al.[18]

To discriminate between the different routes in the initial stages of the reaction, a transient technique, namely temporal analysis of products, was employed. No significant C_{3+} production was observed when pulsing ethanol over H-ZSM-5 owing to incomplete ethanol conversion. In contrast, when pulsing ethene, all of the olefinic products (C_3–C_6) are already observed from the first pulse onwards, as shown in Figure 4a,b. Quantum-chemical calculations (Supporting Information, Figure S3) show that the rate coefficient for the dimerization of ethene is about a hundred times smaller than that for the reaction of ethene with chemisorbed 1-butene. These calculations illustrate that the dimerization of ethene to 1-butene (Route I in Figure 1) can easily be bypassed once sufficient surface species other than the primary C_2H_4* have been formed (Route II or III), hence explaining the autocatalytic behavior. No aromatics are observed during the first pulse. The same olefinic products are still being formed after 25 pulses (Figure 4c,d) but now

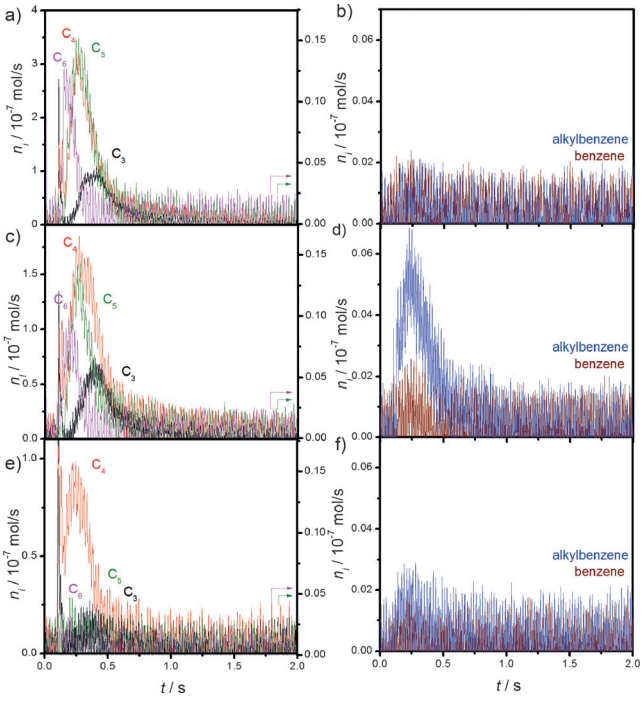

Figure 4. a),b) Response to first ethene pulse, c),d) response to 25th ethene pulse, e),f) response to 400th ethene pulse. Propene (C_3; m/e = 42, black), butenes (C_4; m/e = 56, red), pentenes (C_5; m/e = 70, green), hexenes (C_6; m/e = 84, magenta), benzene (m/e = 78, wine), and alkylaromatics (m/e = 91, blue). ($n_{C_2H_4} = 10^{17}$ molecules/pulse; m_{cat} = 11 mg, T = 648 K).

aromatics are also detected. After 400 pulses (Figure 4e,f), aromatics are no longer observed and only light olefins are produced.

After 400 pulses of ethene, the ethene conversion per pulse decreased to a constant value of ±8% (Figure 5a), which can be related to the formation of surface species blocking the active sites and/or to the formation of coke deposits. The catalyst activity could be restored by simply increasing the temperature to 773 K in the absence of oxygen. This temperature-programmed desorption (TPD) was followed by mass spectrometry, which only detected fragments of m/e = 78 (Figure 5b) and 91. These fragments are repre-

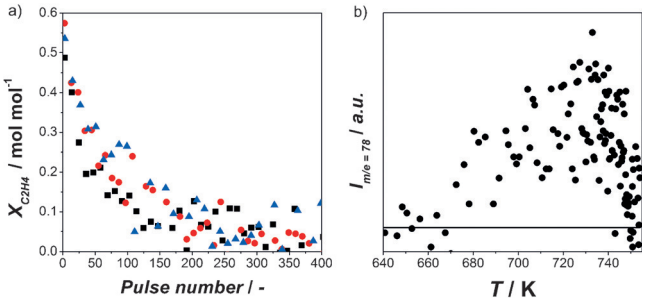

Figure 5. a) Ethene conversion ($X_{C_2H_4}$) as a function of pulse number over fresh H-ZSM-5 (■, black), H-ZSM-5 after reaction and one TPD (▲, blue), H-ZSM-5 after reaction two times, and TPD (■, red), b) Intensity m/e = 78 (benzene) during temperature-programmed desorption (TPD) after treatment of the catalyst with 400 pulses of ethene.

sentative of benzene and alkyl-substituted benzenes, respectively. Also during the TAP experiments, water was found to have little influence (see the Supporting Information).

The nature of the surface species was investigated using UV/Vis spectroscopy of the catalyst used in the continuous-flow experiments. The catalyst bed shows three distinct regions along the reactor axis, as illustrated in Figure 6.

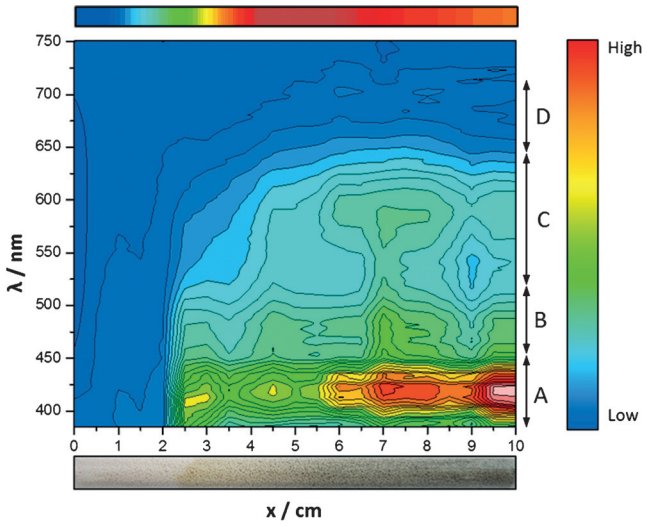

Figure 6. UV/Vis signal as function of wavelength λ and axial reactor coordinate x during continuous feeding of ethanol. Right scale: Color scale ranging from low amount (blue) to high amount (red). Top scale: ethene yield. Bottom picture: catalyst bed with three different zones: $x = 0$–2, $x = 2$–6 and $x = 6$–10 cm. Wavelength ranges are labeled according to Hemelsoet et al.[19] and Mores et al.[20] A) monoalkylaromatics, diaromatics, B) diaromatics, antracenic and phenantracenic structures, C) antracenic, phenantracenic and tetracenic structures, D) polynuclear aromatics (number of aromatics ring > 4; conditions: TOS = 4 h, $T = 573$ K, $p_{EtOH,0} = 30$ kPa).

The absorption wavelengths can be assigned to different types of aromatic compounds.[21] The first zone of the catalyst bed ($x = 0$–2 cm) shows no absorbance, indicating that no aromatic species are retained in the catalyst. This is accompanied by a steep increase in ethene yield and related to ethanol dehydration. At distances from the reactor inlet above 2 cm, absorption starts at wavelengths below 400 nm, reported to be characteristic of monoalkylaromatics.[19] These species correspond to the long-lived surface species C^*_{aro}. When continuing along the reactor coordinate, a redshift from 400 nm towards 420 nm is observed, which is associated with the formation of diaromatics. Simultaneously with this redshift there is increased absorbance at 470 nm, which is related to diaromatics and anthracenic and phenantrenic species. At the end of this zone ($x = 6$ cm), ethene is the major observed gas phase product. In the last zone of the catalyst bed ($x >$ 6 cm), a reduction in ethene yield is observed owing to consecutive reactions. This is accompanied by an increased absorbance around 600 nm, which can be attributed to anthracenic, phenantrenic, and tetracenic species. These species can finally lead to the formation of polynuclear aromatics (absorbance at around 700 nm) on the external surface. The aromatic species can reside inside the catalyst pores for prolonged times due to confinement effects.

The role of the long-lived intermediates, C^*_{aro}, in propene and butene formation was investigated using isotope-labeled ethene. After 400 pulses of $^{13}C_2H_4$, the catalyst was kept under vacuum during 30 s to remove the short-lived surface species before switching the feed to $^{12}C_2H_4$. The evolution of the total ^{12}C content in gas-phase propene and butene after the $^{13}C/^{12}C$ ethene feed switch is shown in Figure 7. Strikingly, butene

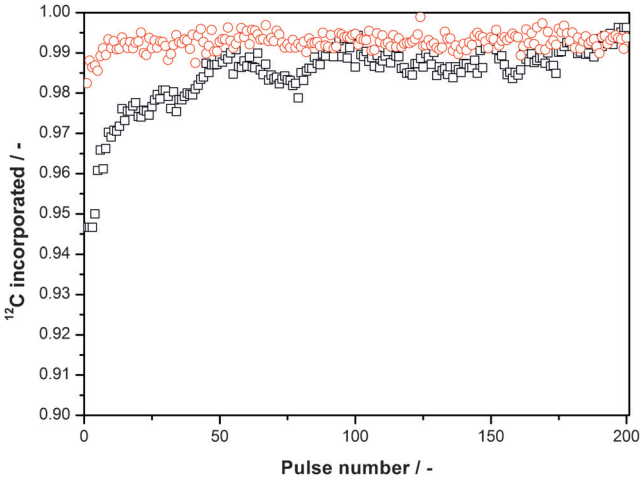

Figure 7. Evolution of the ^{12}C content in propene (□, black) and butenes (○, red) as function of pulse number after switch from ^{13}C labeled ethene feed to ^{12}C labeled ethene.

shows no ^{13}C incorporation, while for propene the ^{13}C uptake amounts to some 5 % and gradually disappears after 50 pulses when complete isotope exchange is approached. These observations suggest that the formation of butenes does not proceed via Route III involving long-lived aromatic surface intermediates (C^*_{aro}), in contrast to propene, but instead mainly occurs through dimerization of ethene (Route I) and further transformation of adsorbed butene via Route II involving fast-produced short-lived aliphatic surface intermediates (C^*_{ali}). Shape-selective effects and steric constraints are apparently prohibiting the formation of specific aromatic intermediates required for the formation of butene via Route III.

Insights in the reaction mechanism, such as the role of dehydration and different surface species, are essential for the development of improved catalysts and process designs. Future work will be directed towards rational catalyst design based on these insights complemented with additional experimentation at high time resolution for complete in-depth understanding of the shape selective phenomena occurring on the catalyst.

Experimental Section

Continuous-flow experiments were performed in a tubular reactor using H-ZSM-5 (Si/Al = 40).[22] The catalyst was diluted with α-alumina (10 wt % H-ZSM-5) to establish a uniform temperature

profile in the catalyst bed. The catalysts were heated to reaction temperature in nitrogen and kept at this temperature for 1 h prior to the reaction. Methane (Air Liquide) was added as an internal standard. It was verified that CH_4, CO, and H_2 were not formed. The carbon balance closed within 5%. The products were analyzed using a GC equipped with a capillary CP-SilPONA column with a temperature program from 223 K to 503 K (ramp: 6 K min^{-1}) and a flame ionization detector. More details related to the temporal analysis of products, UV/Vis spectroscopy, and the computational work can be found in the Supporting Information.

Acknowledgements

The authors acknowledge financial support from the "Long Term Structural Methusalem Funding by the Flemish Government", the Interuniversity Attraction Poles Programme P7/5—Belgian State—Belgian Science Policy. Prof. Dr. Dirk Poelman from the department of Solid State Sciences at Ghent University is acknowledged for his help with the UV/Vis measurements.

Keywords: ab initio calculations · ethanol · isotopic labeling · reaction mechanisms · transient experiments

How to cite: *Angew. Chem. Int. Ed.* **2016**, *55*, 12817–12821
Angew. Chem. **2016**, *128*, 13009–13013

[1] U. Olsbye, S. Svelle, M. Bjorgen, P. Beato, T. V. W. Janssens, F. Joensen, S. Bordiga, K. P. Lillerud, *Angew. Chem. Int. Ed.* **2012**, *51*, 5810–5831; *Angew. Chem.* **2012**, *124*, 5910–5933.

[2] a) E. G. Derouane, J. B. Nagy, P. Dejaifve, J. H. C. Vanhooff, B. P. Spekman, J. C. Vedrine, C. Naccache, *J. Catal.* **1978**, *53*, 40–55; b) J. Sun, Y. Wang, *ACS Catal.* **2014**, *4*, 1078–1090.

[3] H. Xin, X. Li, Y. Fang, X. Yi, W. Hu, Y. Chu, F. Zhang, A. Zheng, H. Zhang, X. Li, *J. Catal.* **2014**, *312*, 204–215.

[4] Z. X. Song, A. Takahashi, I. Nakamura, T. Fujitani, *Appl. Catal. A* **2010**, *384*, 201–205.

[5] a) K. Van der Borght, V. V. Galvita, G. B. Marin, *Appl. Catal. A* **2015**, *492*, 117–126; b) N. R. C. F. Machado, V. Calsavara, N. G. C. Astrath, C. K. Matsuda, A. Paesano Junior, M. L. Baesso, *Fuel* **2005**, *84*, 2064–2070.

[6] a) F. F. Madeira, N. S. Gnep, P. Magnoux, H. Vezin, S. Maury, N. Cadran, *Chem. Eng. J.* **2010**, *161*, 403–408; b) A. T. Aguayo, A. G. Gayubo, A. M. Tarrio, A. Atutxa, J. Bilbao, *J. Chem. Technol. Biotechnol.* **2002**, *77*, 211–216.

[7] A. G. Gayubo, A. M. Tarrío, A. T. Aguayo, M. Olazar, J. Bilbao, *Ind. Eng. Chem. Res.* **2001**, *40*, 3467–3474.

[8] F. F. Madeira, H. Vezin, N. S. Gnep, P. Magnoux, S. Maury, N. Cadran, *ACS Catal.* **2011**, *1*, 417–424.

[9] R. Johansson, S. L. Hruby, J. Rass-Hansen, C. H. Christensen, *Catal. Lett.* **2009**, *127*, 1–6.

[10] a) R. M. Dessau, *J. Catal.* **1986**, *99*, 111–116; b) I. M. Dahl, S. Kolboe, *J. Catal.* **1994**, *149*, 458–464; c) M. Bjørgen, S. Svelle, F. Joensen, J. Nerlov, S. Kolboe, F. Bonino, L. Palumbo, S. Bordiga, U. Olsbye, *J. Catal.* **2007**, *249*, 195–207.

[11] a) D. Lesthaeghe, V. Van Speybroeck, G. B. Marin, M. Waroquier, *Angew. Chem. Int. Ed.* **2006**, *45*, 1714–1719; *Angew. Chem.* **2006**, *118*, 1746–1751; b) D. Lesthaeghe, B. De Sterck, V. Van Speybroeck, G. B. Marin, M. Waroquier, *Angew. Chem. Int. Ed.* **2007**, *46*, 1311–1314; *Angew. Chem.* **2007**, *119*, 1333–1336.

[12] a) H. Yamazaki, H. Shima, H. Imai, T. Yokoi, T. Tatsumi, J. N. Kondo, *J. Phys. Chem. C* **2012**, *116*, 24091–24097; b) H. Yamazaki, H. Shima, H. Imai, T. Yokoi, T. Tatsumi, J. N. Kondo, *Angew. Chem. Int. Ed.* **2011**, *50*, 1853–1856; *Angew. Chem.* **2011**, *123*, 1893–1896.

[13] a) C.-M. Wang, Y.-D. Wang, Y.-J. Du, G. Yang, Z.-K. Xie, *Catal. Sci. Technol.* **2016**, *6*, 3279–3288; b) X. Sun, S. Mueller, Y. Liu, H. Shi, G. L. Haller, M. Sanchez-Sanchez, A. C. van Veen, J. A. Lercher, *J. Catal.* **2014**, *317*, 185–197.

[14] a) M.-F. Reyniers, G. B. Marin, *Annu. Rev. Chem. Biomol. Eng.* **2014**, *5*, 563–594; b) K. Alexopoulos, M. John, K. Van der Borght, V. Galvita, M.-F. Reyniers, G. B. Marin, *J. Catal.* **2016**, *339*, 173–185.

[15] a) T. V. W. Janssens, S. Svelle, U. Olsbye, *J. Catal.* **2013**, *308*, 122–130; b) N. Y. Chen, W. J. Reagan, *J. Catal.* **1979**, *59*, 123–129.

[16] a) V. Bolis, J. C. Vedrine, J. P. Van de Berg, J. P. Wolthuizen, E. G. Derouane, *J. Chem. Soc. Faraday Trans. 1* **1980**, *76*, 1606–1616; b) P. M. Allotta, P. C. Stair, *ACS Catal.* **2012**, *2*, 2424–2432.

[17] N. A. Bhore, M. T. Klein, K. B. Bischoff, *Chem. Eng. Sci.* **1990**, *45*, 2109–2116.

[18] Q. Qian, J. Ruiz-Martínez, M. Mokhtar, A. M. Asiri, S. A. Al-Thabaiti, S. N. Basahel, H. E. van der Bij, J. Kornatowski, B. M. Weckhuysen, *Chem. Eur. J.* **2013**, *19*, 11204–11215.

[19] K. Hemelsoet, Q. Qian, T. De Meyer, K. De Wispelaere, B. De Sterck, B. M. Weckhuysen, M. Waroquier, V. Van Speybroeck, *Chem. Eur. J.* **2013**, *19*, 16595–16606.

[20] D. Mores, J. Kornatowski, U. Olsbye, B. M. Weckhuysen, *Chem. Eur. J.* **2011**, *17*, 2874–2884.

[21] a) D. Mores, E. Stavitski, M. H. F. Kox, J. Kornatowski, U. Olsbye, B. M. Weckhuysen, *Chem. Eur. J.* **2008**, *14*, 11320–11327; b) D. S. Wragg, M. G. O'Brien, F. L. Bleken, M. Di Michiel, U. Olsbye, H. Fjellvåg, *Angew. Chem. Int. Ed.* **2012**, *51*, 7956–7959; *Angew. Chem.* **2012**, *124*, 8080–8083.

[22] K. Van der Borght, K. Toch, V. V. Galvita, J. W. Thybaut, G. B. Marin, *Catalysts* **2015**, *5*, 1948–1968.

Received: July 26, 2016
Published online: September 13, 2016

